Int J Multimed Info Retr (2013) 2:175–188
DOI 10.1007/s13735-013-0037-5

REGULAR PAPER

An intelligent content-based image retrieval system for clinical decision support in brain tumor diagnosis

Megha P. Arakeri · G. Ram Mohana Reddy

Received: 26 December 2012 / Revised: 7 February 2013 / Accepted: 14 February 2013 / Published online: 2 March 2013

Abstract Accurate diagnosis is crucial for successful treatment of the brain tumor. Accordingly in this paper, we propose an intelligent content-based image retrieval (CBIR) system which retrieves similar pathology bearing magnetic resonance (MR) images of the brain from a medical database to assist the radiologist in the diagnosis of the brain tumor. A single feature vector will not perform well for finding similar images in the medical domain as images within the same disease class differ by severity, density and other such factors. To handle this problem, the proposed CBIR system uses a two-step approach to retrieve similar MR images. The first step classifies the query image as benign or malignant using the features that discriminate the classes. The second step then retrieves the most similar images within the predicted class using the features that distinguish the subclasses. In order to provide faster image retrieval, we propose an indexing method called clustering with principal component analysis (PCA) and KD-tree which groups subclass features into clusters using modified K-means clustering and separately reduces the dimensionality of each cluster using PCA. The reduced feature set is then indexed using a KD-tree. The proposed CBIR system is also made robust against misalignment that occurs during MR image acquisition. Experiments were carried out on a database consisting of 820 MR images of the brain tumor. The experimental results demonstrate the effectiveness of the proposed system and show the viability of clinical application.

Keywords Content-based image retrieval · Computer-aided diagnosis · Brain tumor · Classification · Clustering · KD-tree

M. P. Arakeri (✉) · G. Ram Mohana Reddy
National Institute of Technology Karnataka (NITK), Surathkal, Mangalore 575025, India
e-mail: meghalakshman@gmail.com

1 Introduction

Brain tumor is inherently serious and life-threatening because of its invasive and infiltrative character in the limited space of the intracranial cavity. The mortality rates due to the brain tumor are continuously increasing [1]. Brain tumors are mainly classified as benign or malignant depending on their growth pattern. Benign tumors are non-cancerous, slow growing and do not spread to the surrounding tissue. Whereas malignant tumors are cancerous, fast growing and invade nearby organs. Accurate classification of brain tumors is important because their clinical behavior, prognosis and therapy differ markedly. Discrimination between benign and malignant tumors is necessary for optimal patient treatment. The screening tests for the identification of brain tumor require visual examination of MR images of the brain by the radiologist. But visual analysis is time consuming, tedious and subjective. In order to overcome these drawbacks, computer-aided diagnosis (CAD) systems are developed to improve the diagnosis sensitivity by 20–30 % when compared with the diagnosis by visual analysis [2]. Content-based image retrieval (CBIR) is an important component of CAD system which can assist the radiologist in diagnosing tumors. The MR images of patients taken during the diagnosis of the brain tumor are stored in a medical database known as picture archiving and communication system (PACS) along with the diagnosis and treatment information [3]. When the radiologist is less confident about diagnosis of any brain tumor case, he can query a database of past resolved cases to retrieve images that contain regions with features similar to that of the query image. With the knowledge of disease entities that match with the features of the query image and associated diagnostic information, the radiologist can arrive at a diagnostic decision [4]. Thus, the image retrieval helps the radiologist in making case-based

reasoning in diagnosis of brain tumors. Text-based retrieval techniques are now commonly used in PACS. In these systems, keywords from lab reports and associated text from images are used for querying images. Although this approach can offer much flexibility in query formulation, it suffers from several drawbacks such as it is difficult to manually annotate the description of every image in the database and the manual description of the image is subjective due to the difference in human perception [5]. Thus, the text-based retrieval leads to inaccuracies during the retrieval process. Whereas CBIR retrieves similar images from the database based on shape, texture, location and grey level features of the image [6]. This has motivated research and development in CBIR in the medical domain.

1.1 Related work

Content-based image retrieval is a very demanding application in the medical field since it can provide the physician a decision support in the diagnosis of diseases by retrieving relevant cases. The features used to retrieve general images may not apply to medical images. The knowledge of the acquired medical images and disease characteristics is necessary to extract appropriate features of the medical images. Traina et al. [7] present a retrieval system where the shape information about various regions of the brain is extracted to retrieve similar images from the database. The system was not able to retrieve similar images in all the cases as it is based on global features which consider information of the entire image. In medical radiology, the clinically useful information consists of variations in the highly localized region of the image. Hence, attributes characterizing the local regions are required. The pathology bearing region (PBR) has to be segmented on the medical image to extract local features. There exist several brain tumor segmentation techniques such as region-based [8], cluster-based [9] and deformable models [10]. Ahmad et al. [11] experimented with both global features obtained from whole image and local features obtained from non-overlapping image blocks in retrieving similar CT brain images from the database. Retrieval precision of only 94 % was reported since PBR was segmented manually. Automatic segmentation of PBR is necessary in CAD as it is more accurate and consistent.

Color has got limited expressive power in the MR image retrieval as these images are in grey scale. The most vital features of medical images are shape and texture. The shape of the tumor can be characterized with shape descriptors such as Fourier descriptors (FD), Zernike moments and fractals [12]. The malignant brain tumors are more irregular in shape compared to benign tumors. Among the visual features of medical images, texture acquires distinguished importance in identifying tissues. Various texture description methods are proposed in the literature of CBIR such as co-occurrence matrix [13], autoregressive model [14], Tamura [15], wavelets [16] and Gabor filters [17]. Among these methods, multichannel analysis algorithms such as wavelets and Gabor filters have gained a lot of attention due to their ability to characterize features at different frequencies and orientations. The similarity measure used for comparing images in CBIR also has an impact on image retrieval results. Tsang et al. [18] experimented with various similarity measures and achieved a highest precision of 91.7 % with Jeffrey divergence and local texture features. However, good precision was not achieved since tumors were characterized using only texture features.

One of the inherent problems in CBIR is the semantic gap due to the inconsistency between the features extracted and the user interpretation of an image. In the recent years, several methods are proposed to eliminate the semantic gap based on supervised classification, unsupervised classification and relevance feedback [19]. Li-Xin et al. [20] filled the semantic gap by incorporating the relevance feedback into the CBIR system. But, the relevance feedback consumes a lot of time to fine tune the system parameters as it involves the user. K-means clustering is the widely used unsupervised classification method because of its simplicity. However, the K-means algorithm is sensitive to initial cluster centers [21]. Thus, it may give unstable and empty clusters in case of random initialization. There exist several methods for cluster center initialization such as the one based on genetic programming [22], binary splitting [23] and KD-tree [24]. But these methods have increased computational complexity and are parameter dependent. Also K-means clustering requires the user to specify the number of clusters in the data set. This becomes the difficult process if the user does not have any prior knowledge about the data. The existing methods such as the one proposed by Zhao et al. [25], Kothari et al. [26] and Fang et al. [27] solved this problem by running the clustering algorithm for a wide range of clusters and selecting the number of clusters that optimize the cluster validity index. But a single index may not give optimum results in all the cases.

In addition to accuracy, efficiency is also one of the important performance factors to be considered in the development of CBIR system. Thus, the existing CBIR systems make use of various indexing schemes such as KD-tree, R-tree, R*-tree and quad trees to improve the efficiency of the image retrieval system [28]. The indexing techniques retrieve images similar to the query image without comparing each image in the database and thus reduce the retrieval time. All these indexing structures give worst performance in case of large-dimensional feature vectors. Extracting a large number of visual features of an image leads to the dimensionality curse problem, where the indexing, retrieval and similarity matching techniques collapse, due to the fact that it is not possible to well separate the data [29]. Thus, the retrieval accuracy and efficiency can be improved using a feature reduction technique on the feature vector dimensions.

1.2 Motivation

Although several studies are already being conducted with respect to content-based medical image retrieval, many challenging problems still exist:

- Automatic delineation of PBR on the medical image without relying on the radiologist.
- A single feature vector will not perform well in describing tumor because the features that are most effective in discriminating among images from different classes may not be the most effective for retrieval of images belonging to the subclass within a class. That is the hierarchy of classes exists. Benign tumors can be of type Meningioma, Schwannoma, Astrocytoma, etc. Malign tumors can be of type Medulloblastoma, Chrodoma, Neuroblastoma, etc. Thus, to retrieve most similar pathology bearing MR images of the brain tumor there is a need to represent the class and subclass of the tumor.
- Elimination of the semantic gap by developing a CBIR framework that learns well the similarity between the images and inherent structure of the data.
- Making the CBIR system robust to misalignments of images that occur during MR image acquisition.
- Providing efficient indexing structure for faster retrieval of images from the database.
- Proper incorporation of the dimensionality reduction techniques into the CBIR system so that the indexing structures can be beneficial.

Motivated by these needs, in this paper, we propose a CBIR system for automatic extraction and analysis of the tumor region on MR images. The semantic gap between the high- and low-level features is reduced by developing a hierarchical framework that combines supervised and unsupervised classification techniques with different set of tumor features at each level. Also, the system is made efficient by applying modified K-means clustering on the feature set and adopting the indexing structure in low-dimensional feature space.

The rest of the paper is organized as follows: Sect. 2 gives the description of the proposed methodology. The experimental results and performance analysis are presented in Sect. 3. Finally, Sect. 4 concludes the paper.

2 Proposed methodology

The block diagram of the proposed CBIR system for the diagnosis of brain tumor is shown in Fig. 1. It consists of two phases: database building (off-line) and query processing (on-line) phase. In the off-line phase, MR images of the brain tumor stored in the image database are preprocessed by image denoising and rotation correction of misaligned images. Next, images are segmented automatically using wavelet transform and modified fuzzy c-means (MFCM) clustering to identify the brain tumor region on MR images. The segmented tumor is represented using class and subclass features describing the shape and texture of the tumor. Tumor class features are fed to the ensemble classifier consisting of support vector machine (SVM), artificial neural network (ANN) and k-nearest neighbor (k-NN) classifiers to obtain the class label as benign or malignant. The class label along with the subclass features are stored in the feature database. Features in the database are indexed using the proposed clustering with PCA and KD-tree (CPKD) indexing technique. A CPKD structure is constructed with three steps: partitioning the subclass features using the proposed modified K-means clustering, performing local dimensionality reduction by applying PCA to each cluster separately and constructing KD-tree index for the reduced space. Local dimensionality reduction is

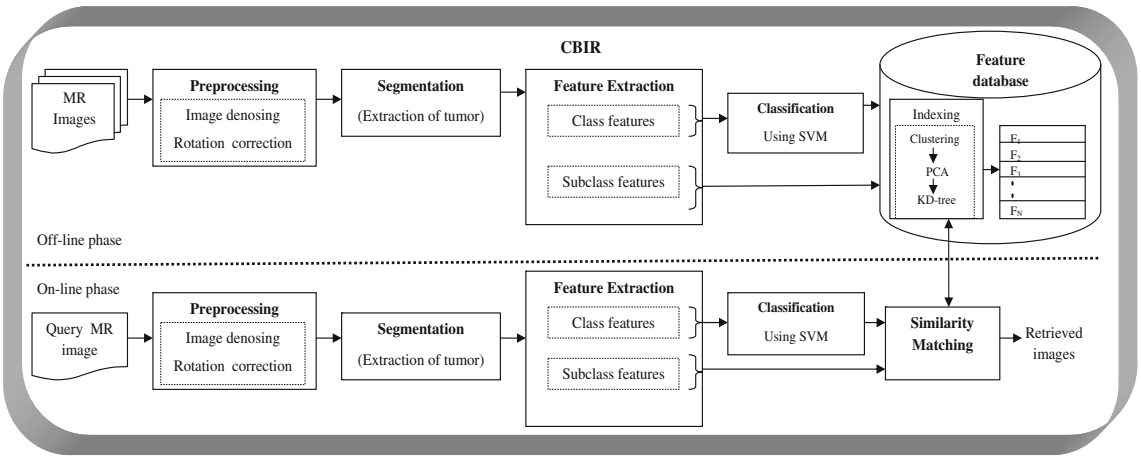

Fig. 1 Framework of the proposed CBIR system

performed within each cluster independently as features are correlated at a local rather than at a global level.

Similarly in the online phase, a query image is preprocessed and segmented. Then, the segmented brain tumor is represented using its class and subclass features. The features of the query image are compared with the features in the database using the Euclidian distance and Chi-square distance as these distance measures are more effective in finding similarity between tumors. The database is indexed using CPKD technique and the most similar pathology bearing MR images of brain tumor are retrieved.

2.1 Problem formulation

Let $D = X_i | i = 1, 2, \ldots N$ be the collection of feature vectors in the database representing N brain tumor MR images. Each feature vector X_i is M-dimensional vector denoted as $X_i = f_j^q | j = 1, 2, \ldots M$. Let Q be the query image with M-dimensional feature vector represented as $f_l^Q | l = 1, 2 \ldots M$. The aim of this paper is to retrieve accurately and efficiently K MR images of brain tumor from the database that are most similar to the query image Q according to similarity distance measure $D(Q, D)$.

2.2 Preprocessing

Medical images are often corrupted by noise during the image acquisition process. The presence of noise in medical image obscures the important information present in the image and hence makes the image analysis task difficult. In the proposed system, the quality of the image is improved by eliminating the noise from the image using 3×3 median filter. Median filter results in smoothing of edges in the image. Hence, to improve the perceptibility of structures in the brain, unsharp masking was used after median filtering. A 3×3 unsharp filter was constructed using the negative of two-dimensional Laplacian filter.

During MR image acquisition, there can be misalignment of images due to movement of the patient. The misalignment results in rotation or translation of the image. The translation will not cause problems in image analysis because the brain tumor can be segmented and analyzed irrespective of the location of brain region in the MR image. But image rotation limits the application of automated tools for MR image analysis as it changes the shape and texture properties of the tumor. Thus, in this work we propose a method for rotation correction of misaligned brain MR images. First, the orientation of the brain image must be identified to know the angle by which to rotate the misaligned image to its standard position. This is accomplished by measuring the orientation of the major axis of the MR image with the reference x-axis as shown in Fig. 2.

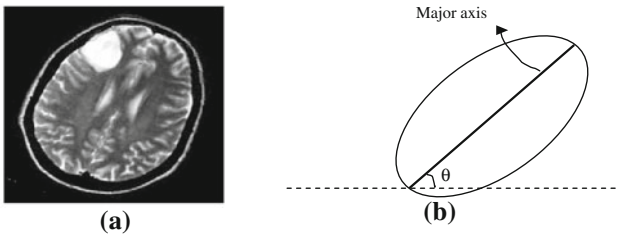

Fig. 2 Orientation angle estimation of the brain MR image. **a** Original brain MR image **b** orientation angle

Then based on the orientation angle (θ), the rotation correction angle ($\theta' = 90 - \theta$) is computed. Then, the misaligned image can be restored to its standard position using the following rotation transformation equations:

$$x' = x\cos(\theta') - y\sin(\theta') \quad (1)$$

$$y' = x\sin(\theta') + y\cos(\theta') \quad (2)$$

where, a point (x, y) in the original image is directly mapped onto the point (x', y') in the resultant image. But, this kind of forward mapping creates holes in the output image as the target position (x', y') does not coincide with the discrete grid points. Thus, to retain the quality of the resultant image, we perform inverse mapping where for each discrete pixel position in the output image, the corresponding continuous position (x, y) is computed in the input image. This mapping hits the non-integer locations in the input image where there is no pixel present. Hence, the pixel value at this non-integer location is computed using interpolation method. In this work, bicubic interpolation method is used as it is more accurate compared to nearest neighbor (NN) and bilinear interpolation techniques [30]. Bicubic interpolation determines a new pixel value by considering nearest 4×4 neighborhood of known pixels and by giving all the 4×4 pixels a weight using their distance to the new pixel. The interpolated pixel value is mapped back to the point (x', y') in the output image.

2.3 Segmentation

Skull removal of the brain in MR image is an important preliminary step in segmentation since it may cause misclassifications of pixels due to intensity similarities with the brain regions. Thus, skull region is eliminated by first converting the original MR image (Fig. 3a) to binary image using Otsu's method [31]. The resultant image consists of connected components as shown in Fig. 3b. Then, a search is made for the largest connected component which corresponds to the brain. Thus, the skull region is eliminated by retaining only the pixels in the largest connected component as shown in Fig. 3c.

Next, the brain tumor is extracted by applying our previously proposed automatic segmentation technique consisting of wavelet decomposition and MFCM clustering [32].

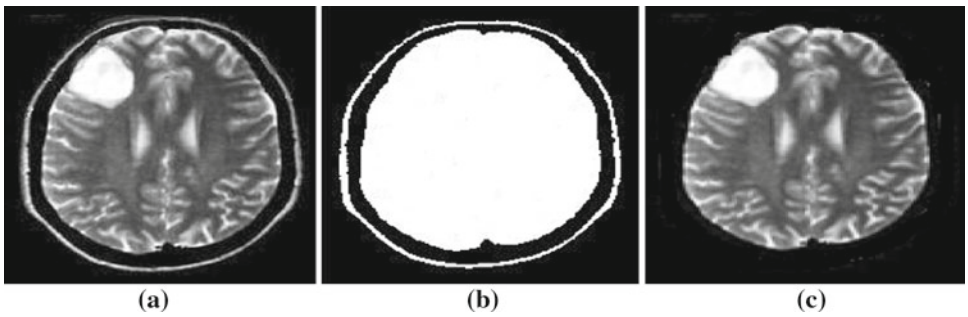

Fig. 3 Brain skull stripping: **a** original MR image **b** binary image **c** skull-stripped image

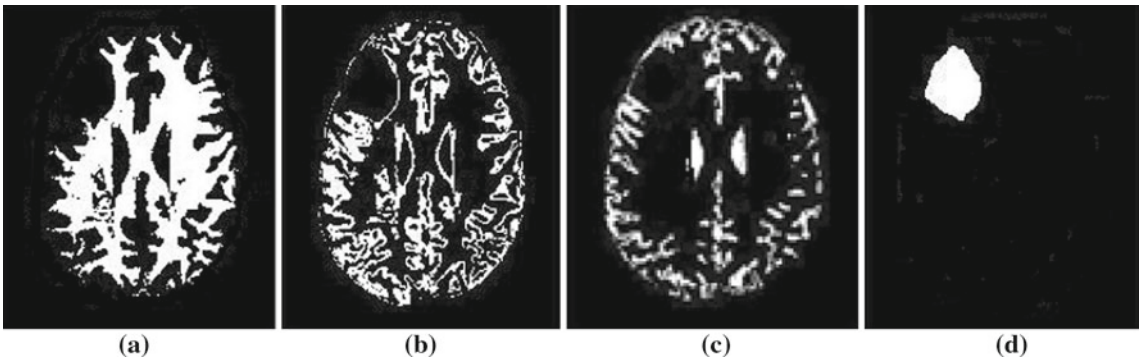

Fig. 4 Brain image clusters **a** white matter **b** grey matter **c** cerebrospinal fluid **d** tumor

The brain image is partitioned into four clusters such as white matter (WM), grey matter (GM), cerebrospinal fluid (CSF) and brain tumor using a fuzzy membership function as shown in Fig. 4. Then, the region of the brain tumor is marked on the MR image by applying 4-connected neighbors.

2.4 Tumor class characterization

In this work, we extracted both 2D and 3D features from the tumor to evaluate their effectiveness in differentiating between benign and malignant tumors. Given a set of slices, the slice containing the largest cross-sectional area of the tumor is chosen as a representative slice of the tumor since it contains the maximum possible information of the tumor. A representative slice was selected from both T1-weighted post contrast and T2-weighted MR images. Instead of processing all slices, a set of 2D features was extracted from a single representative slice to have a faster analysis of the tumor. 3D features were extracted from the 3D model of the tumor which was developed by applying the marching cubes algorithm [33] on a set of slices containing the tumor. The following features were extracted from the representative slice and 3D model of the tumor.

2.4.1 Shape features

Tumor shape is one of the discriminating features for distinguishing between benign and malignant tumors. In this paper, tumor geometric parameters such as circularity, radial length, compactness and fractal dimension are measured to identify the shape of the tumor [34–36].

2.4.2 Texture features

Tissues are expected to have consistent and homogeneous texture along with the series of slices. Therefore, texture information can be used to discriminate among organ tissues. Texture features are extracted using first- and second-order statistics of the tumor region.

First-order statistics In our experiment, five features were calculated from the histogram of the segmented tumor. These features correspond to the average grey level, standard deviation, entropy, skewness and kurtosis [37].

Second-order statistics The texture characteristics which correspond to second-order statistics were derived from the grey level co-occurrence matrix (GLCM) [38]. In case of 2D, four co-occurrence matrices are computed by considering the inter pixel distance of 1 and four angular directions. In case of 3D, 13 co-occurrence matrices are computed by considering the inter voxel distance of 1 and 13 angular directions [39]. Seven features corresponding to contrast, correlation, variance, inverse difference moment, entropy, homogeneity and cluster tendency were extracted from each GLCM to represent the texture of the brain tumor. The texture information on each sub band is represented by taking the average value of each feature computed over all directions.

2.5 Tumor subclass characterization

In medical domain, not all pairs of images within one class have equivalent perceptual similarity. That is a subclass of the tumor exists. Hence, subclass features of the tumor are extracted from the representative slice and 3D model using Fourier descriptors, Gabor filter and edge histogram descriptors (EHD).

2.5.1 Shape feature extraction

The local shape of the tumor is represented using wavelet-based FD [40] as they help in identifying most similar shapes from the database by taking into account the fine details of the shape. Let the boundary coordinates of the tumor be $C(t) = \{(x(t), y(t)), t = 0, 1, \ldots L-1\}$ as shown in Fig. 5. The shape signature of the boundary points is computed using centroid distance function as given in Eq. 3.

$$r(t) = [(x(n) - x_c)^2 + (y(n) - y_c)^2]^{\frac{1}{2}} \tag{3}$$

where,

$$x_c = \frac{1}{L}\sum_{n=0}^{L-1} x(n), \quad y_c = \frac{1}{L}\sum_{n=0}^{L-1} y(n) \tag{4}$$

Next, the wavelet transform is applied on the shape signature, $(r(t))$ as given in Eq. 5. Experiments were carried out with several wavelet functions and Mexican hat wavelets performed better than others. Thus in this work, we use Mexican hat wavelets (φ). Wavelet transform achieves multi-scale representation of the tumor boundary by decomposing it on different levels. Hence, wavelet-based methods are ideally suited for highlighting local features in the decomposed sub-images.

$$C_a(b) = \frac{1}{\sqrt{|a|}}\int_R r(t)\varphi\left(\frac{t-b}{a}\right) \mathrm{d}t \tag{5}$$

where, $C_a(b)$ are wavelet coefficients at scale a and position b. Fourier descriptors are then obtained by applying Fourier transform on wavelet coefficients which is given as:

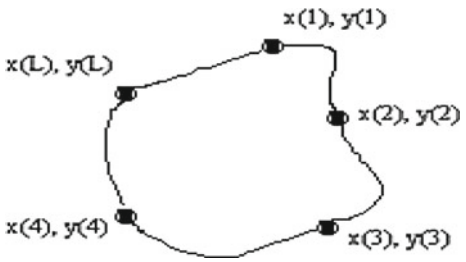

Fig. 5 Boundary points on the brain tumor

$$a_n = \frac{1}{N}\sum_{b=0}^{N-1} C_a(b)\exp(-j2\pi b/N) \tag{6}$$

The Fourier coefficients, a_n, are called FDs of the shape. The shape of the tumor is represented with the feature vector consisting of tumor area and FDs as given below:

$$FS = [A, FD_1, FD_2, \ldots FD_{N-1}]. \tag{7}$$

The first coefficient of the FD is ignored to make shape representation invariant to the boundary starting point.

2.5.2 Texture feature

Local texture of the tumor is extracted using Gabor filter and EHD which are provided by the MPEG-7 standard [41]. These features provide perceptual representation of the image texture and thus help in retrieving most similar images from the database. The Gabor filter extracts the homogeneous texture of the image and EHD represents the local distribution of edges in the image.

Gabor filter Texture analysis of the brain tumor was performed by applying a bank of scale and orientation selective Gabor filters on the tumor image. A 2D Gabor function $g(x, y)$ is given as:

$$g(x, y) = \frac{1}{2\pi\sigma_x\sigma_y}\exp\left[-\frac{1}{2}\left(\frac{x^2}{\sigma_x^2} + \frac{y^2}{\sigma_y^2}\right) + 2\pi j W x\right] \tag{8}$$

where, W is the modulation frequency and σ_x^2 and σ_y^2 represent variance in x and y directions, respectively. A set of self-similar Gabor functions, $g_{mn}(xy)$, are obtained by dilation and rotation of mother Gabor filter using the generating function:

$$g_{mn}(x, y) = a^{-2m} g(x', y'),\ a \geq 1 \tag{9}$$

$$x' = a^{-m}(x\cos(\theta) + y\sin(\theta),$$

$$y' = a^{-m}(-x\sin(\theta) + y\cos(\theta)) \tag{10}$$

where $\theta = \frac{n\pi}{N}$, $m = 0, 1 \ldots M-1$, $n = 0, 1, \ldots N-1$ and a is the scale factor. The parameters M and N specify the total number of scales and orientations, respectively. Based on the experiments, four scales $(M = 4)$ and six orientations $(N = 6)$ were chosen to describe the tumor texture. Texture features of an image $I(x, y)$ are obtained by convolution of $I(x, y)$ with Gabor filter $g_{mn}(x, y)$:

$$G_{mn}(x, y) = I(x_1, y_1) g_{mn}(x - x_1, y - y_1) \tag{11}$$

The mean and the standard deviation of the filtered images, which are used to construct a feature vector, are computed using Eq. (12) and Eq. (13) respectively.

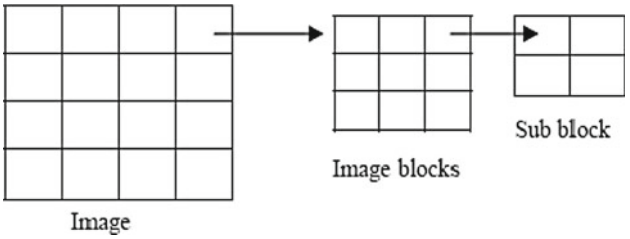

Fig. 6 Image partitioning for EHD computation

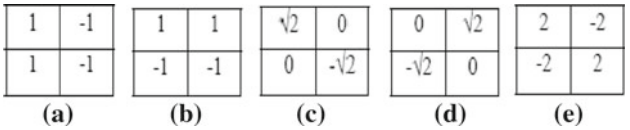

Fig. 7 Edge detection operators: **a** vertical **b** horizontal **c** 45° anti-diagonal **d** 135° diagonal **e** non-directional

$$\mu_{mn} = \frac{1}{P \times Q} \sum_x \sum_y |G_{mn}(x, y)| \tag{12}$$

$$\sigma_{mn} = \sqrt{\frac{1}{P \times Q} \sum_x \sum_y (|G_{mn}(x, y)| - \mu_{mn})^2} \tag{13}$$

where $P \times Q$ is the total number of image pixels. The texture feature vector for M scales and N orientations is given by:

$$\text{FTG} = [\mu_{00}, \sigma_{00}, \mu_{01}, \sigma_{01} \ldots \mu_{(M-1)}, \sigma_{(N-1)}] \tag{14}$$

Edge histogram descriptor EHD represents the local distribution of edges on five different orientations: vertical, horizontal, 45° anti-diagonal, 135° diagonal and non-directed. EHD is computed by dividing the image into 4×4 non-overlapping blocks as shown in Fig. 6. This image partitioning yields 16 equal sized sub-images. Each sub-image is divided into number of image blocks and the image block is divided into four sub-blocks for abstracting the edge histogram.

The edge histogram information is obtained by applying five types of edge detectors defined by MPEG-7 on each sub-block as shown in Fig. 7. This computation results in edge histogram with $16 \times 5 = 80$ bins.

The edge histogram feature vector is represented with the bins of the edge occurrence histogram as given below:

$$\text{FTE} = [B1, B2, \ldots B80] \tag{15}$$

2.6 Classification

The classification stage determines the class of the given sample based on the class features extracted using global shape descriptors, image histogram and GLCM. To overcome the limited generalization performance of single classifier, we use ensemble classifier which combines the decision of multiple classifiers (SVM, ANN, k-NN) to predict the class

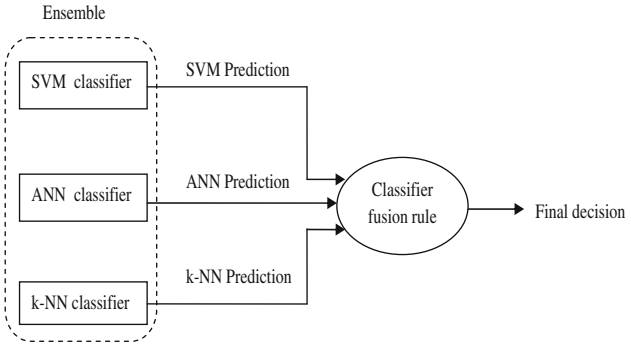

Fig. 8 Framework of ensemble classifier

of the given brain tumor as benign or malignant as shown in Fig. 8.

Ensemble classifier not only improves the classification accuracy but also reduces the chance of over training. This is because the fusion of decision from multiple classifiers avoids a biased decision. The class label obtained using ensemble classifier, along with the subclass features and high-level data of the patient like age and gender, is stored in the feature database.

2.7 Similarity matching

In order to retrieve similar pathology bearing MR images of the brain tumor from the database, the following similarity measures are used to measure the similarity between subclass features of the query image and database images belonging to the same class. The shape similarity between two images x and y is given by the Euclidian distance:

$$\text{DS}(x, y) = \sqrt{(A^x - A^y)^2 + \left(\sum_{i=0}^{N-1} (\text{FD}_i^{(x)} - \text{FD}_i^{(y)})^2 \right)} \tag{16}$$

Where, A and FD represent the area and Fourier descriptors of the tumor, respectively. The texture similarity between two images x and y, with their texture feature vectors obtained by Gabor filter, is measured using the Euclidian distance:

$$\text{DTG}(x, y) = \sum_m \sum_n d_{mn}(x, y) \tag{17}$$

$$d_{mn}(x, y) = \sqrt{(\mu_{mn}(x) - \mu_{mn}(y))^2 + (\sigma_{mn}(x) - \sigma_{mn}(y))^2} \tag{18}$$

where, μ_{mn} and σ_{mn} are mean and standard deviation of the Gabor filtered image at scale m and orientation n. The texture similarity measure between two images x and y, with their texture feature vectors obtained by EHD, is given by the Chi-square distance:

$$\text{DTE} = \chi^2(x, y) = \sum_{k=1}^{K} \frac{[B_x(k) - B_y(k)]^2}{[B_x(k) + B_y(k)]} \tag{19}$$

where, $B_x(k)$ and $B_y(k)$ are kth EHD histogram bin of the image x and y respectively. All the similarity measures are normalized and fused to form a single similarity measure as:

$$D(Q, R) = \mathrm{DS}(x, y) + \mathrm{DTG}(x, y) + \mathrm{DTE}(x, y) \quad (20)$$

In order to retrieve K most relevant images from the database, the calculated distances are sorted in ascending order and corresponding images are retrieved.

2.8 Feature database indexing

Instead of exhaustively matching the features of the query image with all features in the database, a smarter way is to use indexing for faster retrieval. Hence, we propose an indexing method called CPKD which supports efficient processing of NN queries as shown in Fig. 9. Since the subclass labels of tumors are unavailable, the CPKD technique groups subclass features into clusters using the proposed modified K-means clustering (unsupervised classification).

Since the dimensionality of the subclass feature vector is large consisting of 134 features, we need to apply dimensionality reduction technique to reduce the computational complexity and database size. The dimensionality of each cluster is reduced separately using PCA as features are correlated at the local, rather than at the global level. Then within each cluster, the features are indexed using a KD-tree as KD-tree provides searches with $O(\log N)$ efficiency on low-dimensional feature vector.

Given a query image, its similarity to clusters in the database is measured by computing the distance between the query subclass features and the cluster centroids (CT). The query image is considered as the most similar to the cluster with the closest centroid. The query is projected onto the subspace in the nearest cluster. The K-nearest neighbor search is performed on the KD-tree to obtain a subset of K images which are nearest to the query image. The subset contains all the tumor images satisfying (for all $i \in K$),

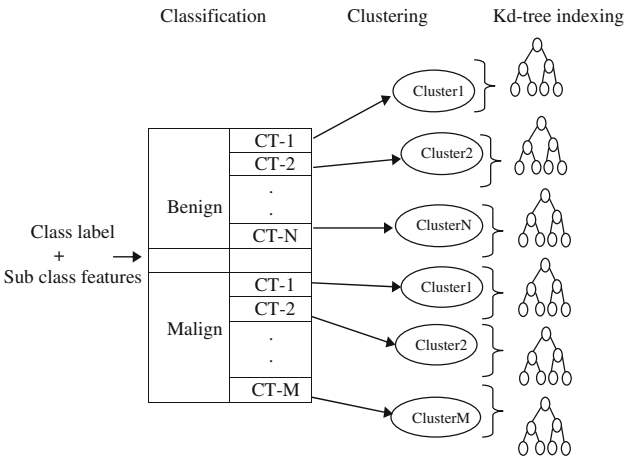

Fig. 9 Index structure for faster retrieval of MR images of brain tumor

$$\| q - i \| < \| q - n \|, \quad \text{for all } n \in (\mathrm{DB} - K) \quad (21)$$

where $\| \cdot \|$ is a distance measure. The KD-tree is a binary search tree which is built from the given feature set by recursively partitioning the tree into two halves at each level based on the median of the dimension having the largest variance. KD-tree reduces the search time by almost eliminating half of the tree during the searching process [42].

2.8.1 Modified K-means clustering

The proposed CPKD indexing structure makes use of the proposed modified K-means clustering to partition the subclass features into different clusters. The main drawback of K-means clustering [43] is its sensitivity to the cluster center initialization and the number of clusters. Since we do not have a prior knowledge on tumor subtypes present in the data set, it is not possible to predict the correct number of clusters. In order to overcome these drawbacks, we propose a method for determining the number of clusters and initial cluster centroids for K-means clustering.

Determining number of clusters We approach the problem of estimating the optimal number of clusters based on the fusion of several validity indexes $V = [V_1, V_2, \ldots V_n]$ value instead of single validity index. The proposed algorithm is as follows:

Algorithm 1 Estimate_Clusters

Input: Tumor subclass features set.
Output: Number of clusters in the feature set.
1: Choose the range of clusters with $C_{\min}$ and C_{max}.
2: **for** $c = C_{\min}$ to $C_{\max}$ **do**
3: Initialize c cluster centers.
4: Apply K-means algorithm to update the membership matrix and the cluster centers (c).
5: Test for convergence. If not converged go to step 4.
6: Compute value of validity indexes $V(c) = [V_1, V_2 \ldots V_n]$.
7: **end for**
8: Normalize values of validity indexes in V.
9: Combine the normalized values using median-based decision fusion to obtain single index, $I(c)$.
10: Choose number of clusters that give optimum value of index, $I(c)$.

The K-means clustering algorithm was applied to the dataset with the number of clusters varying within the range $[C_{\min}, C_{\max}]$. At the end of each run, the partitions of the data set obtained were evaluated using Dunn [44], Davies–Bouldin [45] and Jagota index [46]. Then, min–max normalization was performed to scale the values of validity indexes to the range [0, 1]. The maximum value of Dunn index and minimum value of Davies–Bouldin and Jagota index indicates the best clustering solution. Thus to have consistency, the value of Dunn index is reversed to have a minimum value as an indicator of best partition. Finally, the values of each

run are combined using median-based fusion and the optimal number of clusters is chosen as the one with a minimum fused index value.

Cluster center initialization Clustering is considered as optimal if it minimizes the intra-cluster distance and maximizes the inter-cluster distance. Thus, we base the choice of initial centroids on dissimilarity measure. For a given K clusters, the first two cluster centers chosen are the data items which are located far apart. Next center is chosen as the data item that is farthest from its nearest cluster center. This process is repeated until the desired number of cluster centers is chosen. The proposed algorithm is given in Algorithm 2 (ClusterCenter_Init).

Algorithm 2 ClusterCenter_Init

Input: Number of clusters, Tumor subclass features set.
Output: Cluster centroids.
1: Let $S = 0, 1, \ldots N-1$ represent the data set.
2: For each $(i, j) \in S^2$, compute $d_{ij} = dist(x_i, x_j)$
3: $(i^*, j^*) = \arg\max_{(i,j)\in S^2} d_{ij}$
$C_1 = i^*$
$C_2 = j^*$
$S = S - \{i^*\} - \{j^*\}$
4: **repeat**
5: For each $h \in S$, compute $dist(h, \{C_1, C_2, \ldots C_k\})$.
6: Choose the data item that is farthest from the nearest cluster as the next cluster.
7: $C(k+1) = farthest\_item.$
8: $S = S - \{farthest\_item\}.$
9: **until** $k \neq Number\ of\ clusters$

3 Experimental results and discussion

The proposed method is implemented using MATLAB. All the experiments were performed on a personal computer with 3GHz Pentium processor and 3GB of memory running under Windows XP operating system.

3.1 Dataset

The input dataset consists of the T1-weighted post-contrast and T2-weighted brain MR images of 820 patients (male 438, female 382) with verified and untreated tumors. The patients' ages were in the range of 15–74 years (mean age 48 years). The images were acquired from 1.5-T MRI clinical scanner at Shirdi Sai Cancer Hospital, Manipal, India over the time period of February 2008 to March 2011. The scan of each patient produced set of 64 slices with each slice having a thickness of 2 mm. All images in the data set were grey-scale images with size 640 × 480 and each pixel size corresponds to 0.11 mm × 0.11 mm. Tumors were from 4 to 41 mm in size (mean size 21 mm). Among 820 patients, 420 patients were diagnosed with benign tumor and 400 patients with malignant tumor based on histopathology analysis of biopsy samples. T1-weighted post-contrast and T2-weighted MR images were used in the experiments as they provide important diagnostic information and appreciable contrast between brain regions.

3.1.1 Retrieval results

To test the effectiveness of the rotation correction technique, some of the images in the dataset were rotated by 10°, 15°, 20° and 25° in clockwise and anti clockwise directions. In the preprocessing stage, the misaligned images were corrected using inverse mapping and bicubic interpolation. Table 1 shows the average similarity scores between the original images and the rotation corrected images when the rotation was corrected using three interpolation methods. It was observed that similarity increases when the complexity of the interpolation method increases.

The graphical user interface (GUI) for the CBIR system along with the retrieval results for a given query image is shown in Fig. 10. It can be seen that the system retrieves benign tumor images in response to the query image which is also benign. With the help of a GUI, the user can select a query image and the number of images to be retrieved from the database. The retrieved images are ranked by degree of similarity to the query feature vector. The top 12 most similar images are retrieved and displayed along with the patient data in response to the query image. Also, the retrieval results can be refined for detailed analysis based on the age and gender of the patient. The physician can then study the characteristics of the retrieved tumors and also refer diagnosis report to know the tumor type, severity and prescribed treatment of the corresponding cases. All these parameters assist the radiologist in making case-based reasoning in diagnosis of the brain tumor.

3.2 Performance analysis

The performance of proposed CBIR system is evaluated by measuring retrieval accuracy and efficiency.

Table 1 Performance comparison of interpolation methods

Rotation angle	Similarity scores		
	Nearest neighbor	Bilinear	Bicubic
−10°	1.36	0.98	0.00
−15°	2.73	0.76	0.00
−20°	2.98	1.13	0.01
−25°	4.15	1.20	0.01
10°	1.28	0.71	0.00
15°	3.01	1.02	0.01
20°	4.00	2.08	0.02
25°	4.55	2.11	0.02

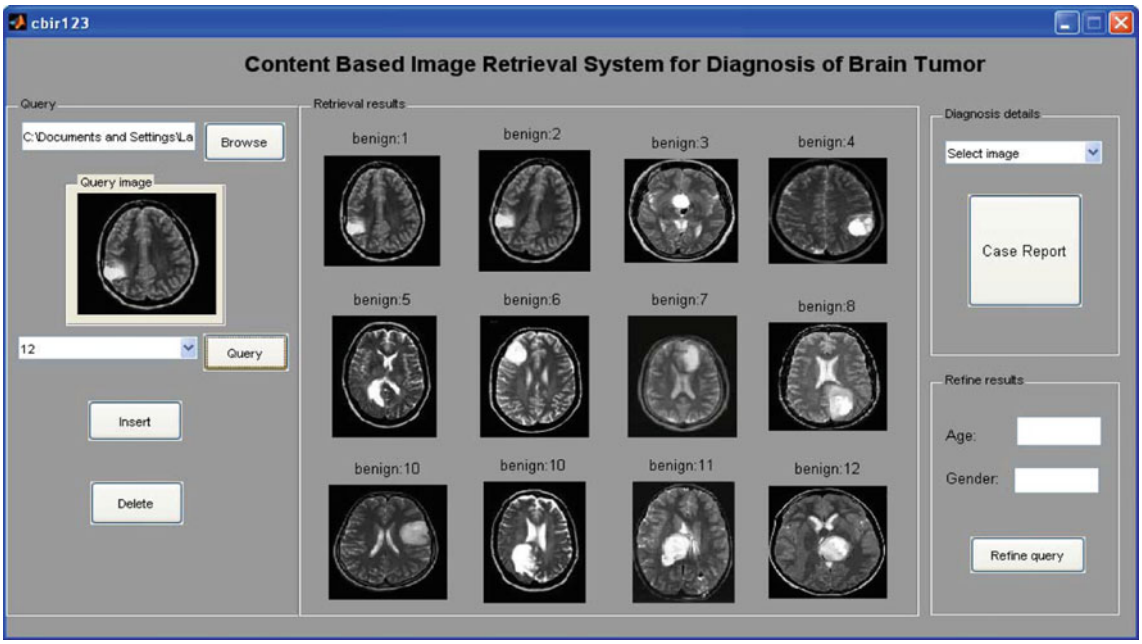

Fig. 10 GUI for content-based image retrieval of brain tumor

3.2.1 Retrieval accuracy

In the classification stage, the ensemble classifier consisting of SVM, ANN and k-NN was used to classify the brain tumor as benign or malignant based on class-specific features. The performance of the ensemble classifier was evaluated using tenfold cross-validation. 820 MR images in the dataset were randomly split into 10 groups with each group consisting of 42 benign tumor and 40 malignant tumor images. Within each iteration, one group was left aside and the ensemble classifier was trained using images of the remaining nine groups. Once trained, the images in the group left aside were tested using the trained ensemble classifier. This process was repeated until every group was tested. Radial basis function was chosen as the kernel function for the SVM classifier. The parameters resulting in optimal classification accuracies consist of the regularization parameter $(C) = 10$ and kernel parameter $(\sigma) = 2.5$ for SVM classifier, eight hidden neurons for ANN classifier and the number of neighbors in k-NN classifier was set as $k = 13$. Table 2 lists the number of misclassified cases in each test set by the ensemble classifier based on 2D and 3D features. It was found that both types of features were equally effective in classifying the brain tumor as benign or malignant.

The performance of the ensemble classifier in tenfold cross-validation is measured using the following performance metrics:

$$\text{Sensitivity} = \frac{\text{TP}}{\text{TP} + \text{FN}} \times 100. \tag{22}$$

$$\text{Specificity} = \frac{\text{TN}}{\text{TN} + \text{FP}} \times 100. \tag{23}$$

Table 2 The number of misclassified cases by ensemble classifier in each test set

Test set	2D features		3D features	
	Malignant	Benign	Malignant	Benign
1	0/40	0/42	0/40	0/42
2	0/40	1/42	0/40	1/42
3	0/40	0/42	0/40	0/42
4	0/40	0/42	0/40	0/42
5	0/40	0/42	0/40	0/42
6	0/40	0/42	0/40	0/42
7	0/40	2/42	0/40	2/42
8	0/40	0/42	0/40	0/42
9	0/40	0/42	0/40	0/42
10	0/40	0/42	0/40	0/42

$$\text{Accuracy} = \frac{\text{TP} + \text{TN}}{\text{TP} + \text{TN} + \text{FP} + \text{FN}} \times 100. \tag{24}$$

where, TP (true positive): number of malignant tumors classified as malignant. FP (false positive): number of benign tumors classified as malignant. TN (true negative): number of benign tumors classified as benign. FN (false negative): number of malignant tumors classified as benign. The accuracy of the ensemble classifier is 99.39 % with 100 % sensitivity and 98.80 % specificity. This means that the ensemble classifier can predict well the malignant category. This is important from the diagnostic viewpoint as the false classification of malignant tumor cases has very serious consequences for the patient. However, some of the benign cases

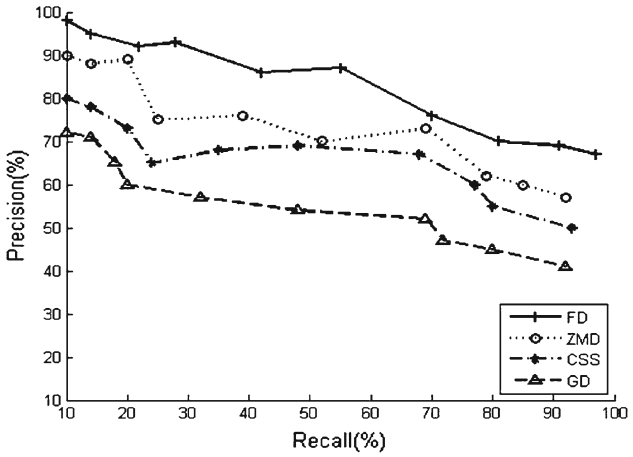

Fig. 11 Performance comparison of shape descriptors

were incorrectly classified due to the difficulty in capturing boundary and shape features of the benign tumors in few cases.

Precision and recall are the standard performance metrics used to measure the effectiveness of the CBIR system in retrieving most similar images. They are computed as:

$$\text{Precision} = \frac{\text{No. of relevant images retrieved}}{\text{No. of images retrieved}} \times 100 \quad (25)$$

$$\text{Recall} = \frac{\text{No. of relevant images retrieved}}{\text{No. of relevant images in the database}} \times 100 \quad (26)$$

The tumor shape description by wavelet-based Fourier descriptors gives a large set of Fourier coefficients representing the tumor contour shape information. Also, since the tumors are of different sizes, the number of boundary points may not be equal. This creates problem in similarity matching. To acquire the knowledge on the number of coefficients necessary for shape matching, we carried out an experiment with 10–30 descriptors. With 10 or 20 descriptors we could obtain the global form of the object but finer details were missing, which are essentially required for better classification. We obtained an optimal tumor shape representation with 30 descriptors. Therefore, we used 30 FDs for tumor retrieval.

The effectiveness of FD in representing tumor shape details is evaluated by comparing it with other state-of-the-art shape descriptors using precision–recall graph as shown in Fig. 11.

Fourier descriptor and curvature scale space (CSS) [47] are contour-based shape descriptors whereas a Zernike moment descriptor (ZMD) and grid descriptors (GD) [48] are region-based shape descriptors. ZMD of MPEG-7 performs better than GD and CSS. However, ZMD loses the important perceptual meaning. FD outperforms in shape representation of tumor compared to other shape descriptors as it applies fourier transform on the wavelet coefficients. Also Fourier descriptors are much easier to derive, match, normalize and more compact compared to other descriptors.

The MPEG-7 Gabor filter and EHD describe homogeneous and non-homogeneous textures of the tumor and perform better when used together for representing subclass of the tumor. The performance comparison of different texture features and combination of texture and shape features for representing the tumor subclass is given in Table 3. It is observed that the 2D and 3D features obtained almost similar retrieval accuracies and the retrieval performance improves when shape descriptors are combined with texture descriptors. Hence, our proposed CBIR system is based on 2D shape and texture features extracted from a representative slice of the tumor instead of 3D model of the tumor built from a set of slices. The proposed combination of shape and texture features extracted using FD, Gabor filter and EHD achieves the highest precision and recall of 98.16 % and 97.35 %, respectively.

In addition to tumor features, the feature similarity measure also has a vital effect on the retrieval results. Thus, we experimented with various similarity measures to evaluate their performance in retrieving similar shapes and texture as shown in Fig. 12. It is found that Euclidian and Chi-square distances give good retrieval performance when used for comparing shape and texture features, respectively.

3.2.2 *Retrieval efficiency*

In order to provide faster retrieval results, the proposed CPKD indexing method prunes the search space by clustering subclass features using the proposed modified K-means clustering algorithm. Table 4 shows the number of clusters determined in the benign brain tumor dataset by the proposed algorithm (Estimate_Clusters). In the experiments, the number of clusters was varied between $C_{\min} = 2$ and $C_{\max} = \sqrt{n}$ based on Bezdek's suggestion [49], where n indicates the number of features to be clustered. For simplicity, only ten entries are shown in the table. The clustering results obtained are evaluated using Dunn, Davies–Bouldin and Jagota index. The minimum fused index value indicates optimal clustering. As shown in the highlighted row of Table 4, the algorithm identifies seven clusters in the benign brain tumor data set, as with this set of clusters the fused value obtained from validity indices is optimized. Similarly, five clusters were identified in the malignant tumor set. We also evaluated the clustering results using the randomly initialized centers and initial centers derived by the proposed algorithm (ClusterCenter_Init) in terms of cluster center proximity (CCP) [48] which is given as:

$$\text{CCP} = \frac{1}{K \times m} \sum_{s=1}^{K} \sum_{j=1}^{m} \left| \frac{f_{sj} - C_{sj}}{f_{sj}} \right| \quad (27)$$

Table 3 Performance comparison of feature descriptors

Feature descriptors	2D features		3D features	
	Precision (%)	Recall (%)	Precision (%)	Recall (%)
Gabor filter	92.52	88.41	92.52	88.41
EHD	90.11	93.53	90.11	93.48
GLCM	85.62	83.0	85.65	83.03
Tamura	82.18	79.31	82.18	79.31
Gabor filter + FD	95.0	94.86	95.0	94.86
EHD + FD	94.72	95.20	94.70	95.20
GLCM + FD	92.55	88.53	92.55	88.58
Tamura + FD	90.60	88.15	99.60	88.15
Gabor filter + EHD + FD (proposed)	98.16	97.35	98.16	97.35

Table 4 Estimation of number of clusters in benign brain tumor data set

No. of clusters	Cluster validity indices			Index fusion
	Dunn	Davies–Bouldin	Jagota	
2	0.85	0.83	0.69	0.83
3	0.80	0.59	0.72	0.72
4	0.68	0.27	0.53	0.53
5	0.38	0.24	0.19	0.24
6	0.16	0.20	0.21	0.20
7	**0.06**	**0.09**	**0.17**	**0.09**
8	0.08	0.14	0.20	0.14
9	0.15	0.21	0.23	0.19
10	0.18	0.27	0.25	0.25

where f_{sj} and C_{sj} indicate jth attribute value of the desired and initial cluster centers, respectively. CCP values of 0.62 and 0.10 were obtained with random and proposed initialization technique, respectively. This infers that the proposed method predicts initial cluster centers nearer to actual cluster centers. Table 5 shows the comparison of time complexity of different indexing methods for processing the nearest neighbor queries on feature database. Where, N and D represent number of feature vectors and their original dimensions, respectively. $N^{(h)}$ and D' represent number of feature vectors in cluster $h(h = 1, 2 \ldots K)$ and their reduced dimensions, respectively. C indicates the number of clusters in the dataset.

It is observed that exhaustive search which is a brute force search method consumes more time to retrieve similar tumor images from the database. Whereas the proposed method takes very less time (2–3 s) compared to other methods. This is because it has a combination of modified K-means clustering, PCA and KD-tree. The use of clustering and PCA prunes the search space by limiting the query to lower dimensionality space of the closest cluster instead of searching the entire database. Also, the KD-tree gives good search performance of $O(\log N)$ in lower dimensional spaces. Thus, the proposed indexing method narrows down the search space and thus accelerates the retrieval task.

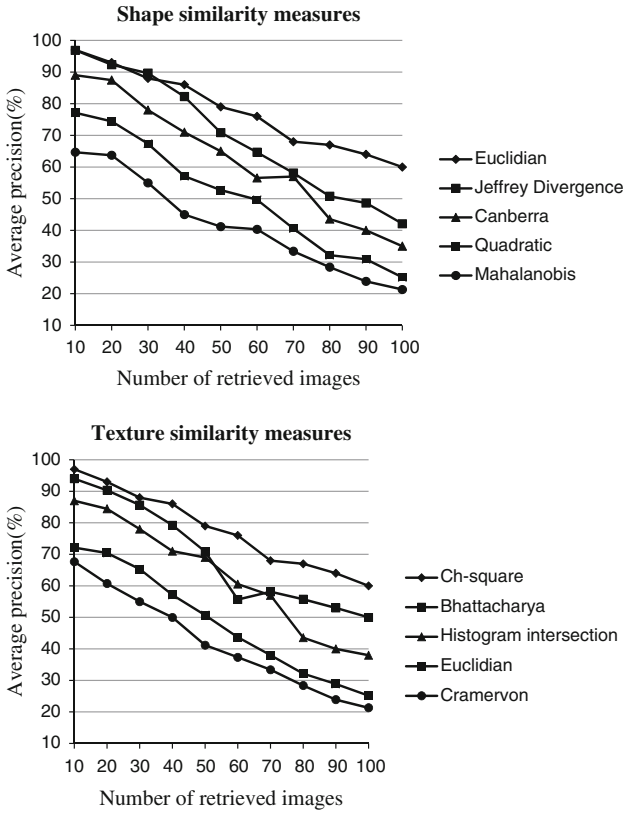

Fig. 12 Comparison of similarity measures

The retrieval performance of the proposed CBIR method was compared with the following existing methods as shown in Fig. 13:

- E1: Retrieval using multiple features (Emmanuel et al. [50]).
- E2: Retrieval based on classification (Dube et al. [51]).
- E3: Retrieval based on machine learning and clustering (Rahman et al. [52]).

Table 5 Comparison of database indexing techniques

Indexing method	Exhaustive search	Clustering	CPKD (proposed)
Retrieval time	$O(DN)$	$O(DC) + O(C) + O(D'N^{(h)})$	$O(DC) + O(C) + O(D' \log N^{(h)})$

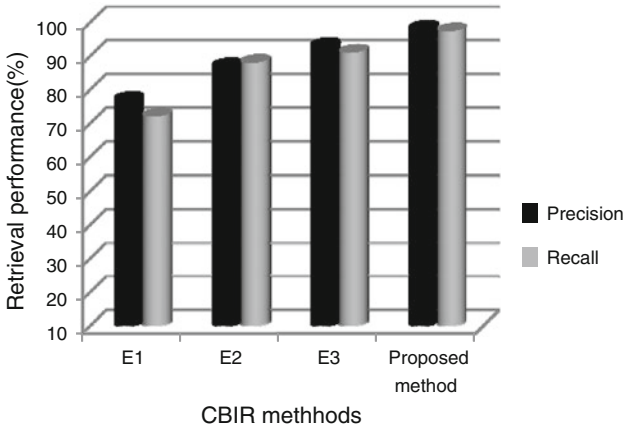

Fig. 13 Performance comparison of CBIR systems

Emmanuel et al. [50] extracted multiple features to characterize the tumor completely. But a large number of features leads to curse of dimensionality problem. Dube et al. [51] retrieved brain tumors based on classification. They reported accuracy of only 87 % as the system could not match the images of subclasses. In order to enhance similarity learning, Rahman et al. [52] combined classification with clustering. But the same feature set was used for both classification and retrieval after classification. Thus, the system could not achieve higher performance in retrieving most similar images. Our proposed method for CBIR fills the semantic gap by learning the similarity hierarchically with different set of features to represent the tumor at each level. Thus, it achieves good precision and recall rates as compared to other CBIR methods.

4 Conclusion

In this paper we have proposed an accurate, efficient and automatic approach to brain tumor diagnosis based on content-based retrieval of MR images from the medical image database. The proposed approach resolves the MR image misalignment problems by rotation correction technique. The system is made accurate by the hierarchical approach to similarity learning and extracting more effective features for representing the brain tumor type. Also, the system is made more efficient by incorporating indexing technique which is developed based on modified K-means clustering, PCA and KD-tree.

The performance evaluation demonstrated that the combination of features yields better retrieval accuracy than using features independently. Also, the various similarity measures were compared to select the measure that retrieves most similar images. The proposed indexing technique proved to be better than the exhaustive search. Overall, the fusion of several features of the tumor and the indexing technique resulted in good retrieval accuracy with 98.16 % precision and 97.35 % recall. Thus, the proposed CBIR system can be used in hospitals for assisting the radiologist in diagnosing brain tumors with good accuracy and speed.

Acknowledgments The authors wish to thank the anonymous reviewers for the useful and valuable suggestions.

References

1. World Health Organization Cancer Fact Sheets. Available[online]: http://www.who.int/mediacentre/factsheets/fs297/en/index.html
2. Stoitsis J, Valavanis I, Mougiakakou SG, Golemati S, Nikita A, Nikita KS (2006) Computer aided diagnosis based on medical image processing and artificial intelligence methods. Nucl Instrum Methods Phys Res 569(2):591–595
3. Yuan K, Feng S, Chen W, Jia S, Xiao P (2008) Diagnosis system of computer aided brain MRI using content based image retrieval. In: Proceedings of international conference on information technology and application in biomedicine, IEEE, pp 152–156
4. Quellec G, Lambard M, Cazuguel G, Roux C, Cochener B (2011) Case retrieval in medical databases by fusing heterogeneous information. IEEE Trans Med Imaging 30(1):108–118
5. Agarwal P, Sardana HK, Jindal G (2009) Content based medical image retrieval: theory, gaps and future directions. Graphics Vis Image Process 9(2):27–37
6. Muller H, Michoux N, Bandon D, Geissbuhler A (2004) A review of content-based image retrieval systems in medical applications—clinical benefits and future directions. Int J Med Inf 73(1):1–23
7. Traina AGM, Balan AGR, Bortolotti LM, Traina C Jr (2004) Content-based image retrieval using approximate shape of objects. In: Proceedings of IEEE symposium on computer-based medical systems, pp 91–96
8. Hamarneh G, Li X (2009) Watershed segmentation using prior shape and appearance knowledge. Image Vis Comput 27(1):59–68
9. Ng HP, Ong SH, Foong KWC, Goh PS, Nowinski WL (2006) Medical image segmentation using k-means clustering and improved watershed algorithm. In: Proceedings of IEEE SouthWest symposium on image analysis and interpretation, pp 61–65
10. MyungEun L, SoonYoung P, WanHyun C (2007) Medical image segmentation using geometric active contour model based on level set method. In: Proceedings of IEEE international conference on communications, computers and signal processing, pp 577–580
11. Ahmad Fauzi MF, Ahmad WSHMW (2008) Efficient block based matching for content based retrieval of CT head images. In: Proceedings of IEEE workshop on multimedia signal processing, pp 142–147

12. Shahabi C, Safar M (2007) An experimental study of alternative shape-based image retrieval techniques. Multimed Tools Appl 32(1):29–48
13. Kassner A, Thornhill RE (2010) Texture analysis: a review of neurologic MR imaging applications. Am J Neuroradiol 31:809–816
14. Castellano G, Bonilha L, Li LM, Cendes F (2004) Texture analysis of medical images. Clin Radiol 59(12):1061–1069
15. Prasad BG, Krishna AN (2011) Statistical texture feature-based retrieval and performance evaluation of CT brain images. In: Proceedings of international conference on electronics computer technology, IEEE, pp 289–293
16. Rajkumar K, Muttan S (2010) Medical image retrieval using energy efficient wavelet transform. In: Proceedings of international conference on computing, communication and network technologies, IEEE, pp 1–5
17. Buciu I, Gacsadi A (2011) Directional features for automatic tumor classification of mammogram images. Biomed Signal Process 6(4):370–378
18. Tsang W, Corboy A, Lee K, Raicu D, Furst J (2005) Texture-based image retrieval for computerized tomography databases. In: Proceedings of IEEE symposium on computer-based medical systems, pp 1–5
19. Trpovski Z (2008) Content based image retrieval: from pixels to semantics. In: Proceedings of symposium on neural network applications in electrical engineering, IEEE, pp 7–12
20. Li-xin S, Rui-feng C, Qian W (2010) Image retrieval of calcification clusters in mammogram using feature fusion and relevance feedback. In: Proceedings of international forum on strategic technology, IEEE, pp 15–18
21. Bishnu PS, Bhattacherjee V (2012) Software fault prediction using quad tree-based K-means clustering algorithm. IEEE Trans Knowl Data Eng 24(6):1146–1150
22. Linde Y, Buzo A, Gray R (1980) An algorithm for vector quantizer design. IEEE Trans Commun 28:84–95
23. Babu GP, Murty MN (1993) A near-optimal initial seed value selection in k-means means algorithm using a genetic algorithm. Pattern Recognit Lett 14(10):763–769
24. Likas A, Vlassis N, Verbeek JJ (2003) The global k-means clustering algorithm. Pattern Recognit 36:451–461
25. Zhao Q, Xu M, Franti P (2011) Extending external validity measures for determining the number of clusters. In: Proceedings of international conference on intelligent system design and applications, IEEE, pp 931–936
26. Kothari R, Pitts D (1999) On finding the number of clusters. Pattern Recognit Lett 20:405–416
27. Fang Y, Wang J (2012) Selection of the number of clusters via the bootstrap method. Comput Stat Data Anal 56:468–477
28. Lu G (2002) Techniques and data structures for efficient multimedia retrieval based on similarity. IEEE Trans Multimed 4(3):372–384
29. Wu Y, Chang EY, Chang KCC, Smith JR (2004) Optimal multimodal fusion for multimedia data analysis. In: Proceedings of ACM international conference on multimedia, pp 572–579
30. Amruta A, Gole A, Karunakar Y (2010) A systematic algorithm for 3D reconstruction of MRI based brain tumors using morphological operators and bicubic interpolation. In: Proceedings of international conference on computer technology and development, IEEE, pp 305–309
31. Otsu N (1979) A threshold selection method from gray-level histogram. IEEE Trans Syst Man Cybern 9(1):62–66
32. Arakeri MP, Reddy GRM (2011) Efficient fuzzy clustering based approach to brain tumor segmentation on MR images. In: Proceedings of computational intelligence and information technology, CCIS, vol 250, issue no 3. Springer, Berlin, pp 790–795
33. Lorensen WE, Cline HE (1987) Marching cubes: a high resolution 3D surface construction algorithm. In: Proceedings of 14th ACM SIGGRAPH annual conference on computer graphics and interactive, techniques, pp 163–169
34. Mingqiang Y, Kidiyo K, Joseph R (2008) A survey of shape feature extraction techniques. In: Yin P-Y (ed) Pattern recognition, pp 43–90
35. Kassimi MA, El beqqali O (2011) 3D model retrieval based on semantic and shape indexes. Int J Comput Sci Issues 8(1):172–181
36. Wu YT, Shyu KK, Jao CW, Wang ZY, Soong BW, Wu HM, Wang PS (2010) Fractal dimension analysis for quantifying cerebellar morphological change of multiple system atrophy of the cerebellar type (MSA-C). Neuroimage 49(1):539–551
37. Akilandeswari U, Nithya R, Santhi B (2012) Review on feature extraction methods in pattern classification. Eur J Sci Res 71(2):265–272
38. Haralick RM, Shanmugam K, Dinstein I (1973) Texture features for image classification. IEEE Trans Syst Man Cybern 3(6):610–621
39. Showalter C, Clymer BD, Richmond B, Powell K (2005) Three-dimensional texture analysis of cancellous bone cores evaluated at clinical CT resolutions. Osteoporos Int 17(2):259–266
40. Kunttu I, Lepisto L, Rauhamaa J, Visa A (2006) Multiscale fourier descriptors for defect image retrieval. Pattern Recognit Lett 27:123–132
41. Manjunath BS, Ohm JR, Vasudevan VV, Yamada A (2001) Color and texture descriptors. IEEE Trans Circuits Syst Video Technol 11(6):703–715
42. Javier H, Jordi N, Marc S (2012) Kd-tree and the real disclosure risks of large statistical databases. Inf Fusion 13(4):260–273
43. Duda R, Hart P, Stork D (2012) Pattern classification, 2nd edn. John Wiley & Sons, pp 526–528
44. Dunn JC (1974) A fuzzy relative of the isodata process and its use in detecting compact and well separated clusters. J Cybern 3(3):32–57
45. Davies DL, Bouldin DW (2000) A cluster separation measure. IEEE Trans Pattern Anal Mach Intell 1(4):224–227
46. Jagota A (1991) Novelty detection on a very large number memories stored in hopified-style network. In: Proceedings of international conference on neural networks, IEEE
47. Mokhtarian F, Ung YK, Wang Z (2005) Automatic fitting of digitised contours at multiscales through the curvature scale space technique. Comput Graphics 29:961–971
48. Lu G, Sajjanhar A (1999) Region-based shape representation and similarity measure suitable for content based image retrieval. Multimed Syst 7(2):165–174
49. Bezdek JC, Pal NR (1998) Some new indexes of cluster validity. IEEE Trans Syst Man Cybern 28:301–315
50. Emmanuel M, Ramesh Babu DR, Potdar GP, Sonkamble BA, Praveen G (2007) Content based medical image retrieval. In: Proceedings of international conference on information and communication technology in electrical sciences, IEEE, pp 712–717
51. Dube S, El-Saden S, Cloughesy TF, Sinha U (2006) Content based image retrieval for MR image studies of brain tumors. In: Proceedings of IEEE international conference on engineering in medicine and biology, pp 3337–3340
52. Rahman MM, Bhattacharya P, Desai BC (2007) A framework for medical image retrieval using machine learning and statistical similarity matching techniques with relevance feedback. IEEE Trans Inf Technol Biomed 11(1):58–69